



Solar cycle variations of the Cluster spacecraft potential and its use for electron density estimations

B Lybekk, A Pedersen, S Haaland, K Svenes, Andrew N. Fazakerley, A Masson, M.G.G.T. Taylor, Jean-Gabriel Trotignon

► To cite this version:

B Lybekk, A Pedersen, S Haaland, K Svenes, Andrew N. Fazakerley, et al.. Solar cycle variations of the Cluster spacecraft potential and its use for electron density estimations. *Journal of Geophysical Research Space Physics*, 2012, 117, A01217 (14 p.). 10.1029/2011JA016969 . insu-01179669

HAL Id: insu-01179669

<https://hal-insu.archives-ouvertes.fr/insu-01179669>

Submitted on 23 Jul 2015

HAL is a multi-disciplinary open access archive for the deposit and dissemination of scientific research documents, whether they are published or not. The documents may come from teaching and research institutions in France or abroad, or from public or private research centers.

L'archive ouverte pluridisciplinaire **HAL**, est destinée au dépôt et à la diffusion de documents scientifiques de niveau recherche, publiés ou non, émanant des établissements d'enseignement et de recherche français ou étrangers, des laboratoires publics ou privés.

Solar cycle variations of the Cluster spacecraft potential and its use for electron density estimations

B. Lybekk,¹ A. Pedersen,¹ S. Haaland,² K. Svenes,³ A. N. Fazakerley,⁴ A. Masson,⁵ M. G. G. T. Taylor,⁵ and J.-G. Trotignon⁶

Received 30 June 2011; revised 6 December 2011; accepted 6 December 2011; published 31 January 2012.

[1] A sunlit conductive spacecraft, immersed in tenuous plasma, will attain a positive potential relative to the ambient plasma. This potential is primarily governed by solar irradiation, which causes escape of photoelectrons from the surface of the spacecraft, and the electrons in the ambient plasma providing the return current. In this paper we combine potential measurements from the Cluster satellites with measurements of extreme ultraviolet radiation from the TIMED satellite to establish a relation between solar radiation and spacecraft charging from solar maximum to solar minimum. We then use this relation to derive an improved method for determination of the current balance of the spacecraft. By calibration with other instruments we thereafter derive the plasma density. The results show that this method can provide information about plasma densities in the polar cap and magnetotail lobe regions where other measurements have limitations.

Citation: Lybekk, B., A. Pedersen, S. Haaland, K. Svenes, A. N. Fazakerley, A. Masson, M. G. G. T. Taylor, and J.-G. Trotignon (2012), Solar cycle variations of the Cluster spacecraft potential and its use for electron density estimations, *J. Geophys. Res.*, *117*, A01217, doi:10.1029/2011JA016969.

1. Introduction

[2] Langmuir probes on early sounding rockets demonstrated that a rocket in the lower ionosphere would achieve a negative potential with respect to the ambient plasma. Only a small high energy fraction of the electron energy distribution would balance the flux of ions. The even smaller flux of photoelectrons will not significantly change this picture. The NASA Explorer and IMP satellites were the first to carry out basic measurements in the magnetosphere, and *Whipple* [1965] was one of the first to conclude that a sunlit spacecraft in the magnetosphere would achieve a positive potential, because the flux of photoelectrons would dominate over the flux of electrons in the thin plasma of the magnetosphere. A current balance could only be achieved by attracting low energy photoelectrons back to the positively charged spacecraft, and allowing only higher energy photoelectrons to escape and be in balance with collected electrons.

[3] *Fahleson* [1967] published a detailed description of an electric field experiment, using spherical double probes. This became the basis for development of electric field experiments in the magnetosphere on GEOS-1, GEOS-2 and ISEE-1 (launch years 1977, 1978 and 1978). These satellites

had surfaces with sufficient conductivity to keep the whole spacecraft at a uniform potential. The potential was measured with reference to electric field probes, kept close to the ambient plasma potential. Several papers have used spacecraft potential measurements on satellites to estimate densities in the magnetosphere [*Pedersen*, 1995; *Escoubet et al.*, 1997; *Laakso and Pedersen*, 1998; *Nakagawa et al.*, 2000; *Pedersen et al.*, 2001; *Scudder et al.*, 2000; *Laakso et al.*, 2002].

[4] *Brace et al.* [1988] published variations of solar EUV radiation during the years 1981–1987, based on negative voltage sweeps on a Langmuir probe on the Pioneer Venus Orbiter, leading to measurements of photoelectrons in addition to collected ions. These measurements, and simultaneous Lyman alpha measurements on Solar Mesospheric Explorer, demonstrated that EUV radiation had a significant variation with solar rotation, as well as a 30–40% drop from solar maximum to solar minimum. However, it was only after years of observations on the Cluster satellites, and modeling of the potential distribution around Cluster [*Cully et al.*, 2007], that it was possible to use spacecraft potential measurements to develop a more accurate method for estimating the electron density in a thin plasma, and to demonstrate that the solar cycle variation of photoelectron emission had to be considered [*Pedersen et al.*, 2008].

[5] This paper is a further development of this method. Data from the Cluster Active Archive has made it possible to obtain qualified data for calibration of the method: Ion data from CIS [*Rème et al.*, 2001], electron data from PEACE [*Johnstone et al.*, 1997], electron density from the plasma wave experiments on WHISPER [*Décrou et al.*, 1997] and WIDEBAND (WBD) [*Gurnett et al.*, 1997]. Certain calibrations have been done during periods when the spacecraft

¹Department of Physics, University of Oslo, Oslo, Norway.

²Max-Planck Institut für Sonnensystemforschung, Katlenburg-Lindau, Germany.

³Norwegian Defence Research Establishment, Kjeller, Norway.

⁴Mullard Space Science Laboratory, University College London, Dorking, UK.

⁵RSSD, ESA-ESTEC, Noordwijk, Netherlands.

⁶CNRS/LPC2E, Orléans, France.

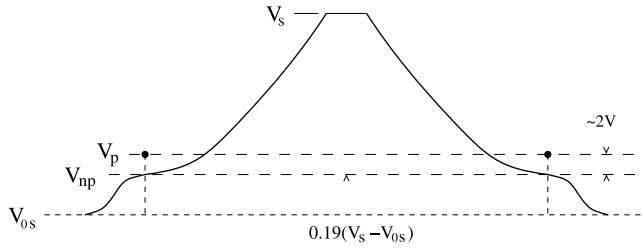


Figure 1. Schematic presentation of the spacecraft potential relative to the ambient plasma, $(V_s - V_{0s})$, and the potentials of the electric field probes, V_p , controlled to be at $(+2 \pm 0.5)$ V relative to their local plasma potential, V_{np} . The spacecraft to probe potential difference, $(V_s - V_p)$, is measured by the electric field experiment EFW.

potential was reduced by ion emission from ASPOC [Torkar et al., 2001]. Furthermore solar EUV data from the TIMED satellite has made it possible to see how short-term and long-term variations of solar photons influence the spacecraft potential.

[6] Calibrations of the method with data from the CIS, PEACE and WHISPER have mainly been carried out on Cluster C4, where all four electric field probes have been in operation for the times considered in this paper. One reason for this choice is that the electron drift experiment, EDI, does not operate on C4. On the other Cluster satellites the EDI electron emission will, at periods with increased emission, influence the spacecraft potential in tenuous plasmas. Furthermore these three satellites, and in particular C3, are less positive than C4 for large spacecraft potentials after 2005. This is probably related to changes in spacecraft conductive surfaces and will be discussed later.

2. Experiment Description, Data Analysis, and Calibrations of the Method

[7] The electric field experiment, EFW, on Cluster has been described by Gustafsson et al. [1997]. Electric field probes are placed at the tips of four radial wire booms, 44 m from the spacecraft spin axis. This separation brings the probes closer to the ambient plasma. However, the probes are influenced by the potential of the boom tips, kept at the spacecraft potential. Details of the probe – boom tip interface and the functioning of the electric field probes are given by Pedersen et al. [2008]. Cully et al. [2007] have developed a model of the potential around a Cluster spacecraft when the Debye length of the undisturbed plasma, λ_D , is large compared to the spacecraft to probe distance of 44 m. Orbiting and escaping photoelectrons influence the potential distribution around the spacecraft and the long booms. In this model the plasma near the electric field probes is approximately 19% of the potential of the spacecraft relative to the undisturbed plasma. The model can be used for tenuous plasma conditions in the lobes, the polar caps and the cusps near the polar caps. Figure 1 is a sketch of the spacecraft potential relative to the undisturbed plasma, $(V_s - V_{0s})$, and the measured potential between spacecraft and probes, $(V_s - V_p)$. The potential of the probes, V_p , is controlled to be

at a small positive potential relative to their local plasma at a potential V_{np} . The model of Cully et al. [2007] gives the potential of V_{np} relative to the undisturbed plasma, and we can write: $(V_{np} - V_{0s}) = 0.19 (V_s - V_{0s})$.

[8] Mott-Smith and Langmuir [1926] presented a formulae for the electron current, I_e , to a conductive sphere at a positive potential, V_b , relative to the undisturbed plasma at a potential V_0 . A condition for the use of this formula is that λ_D is larger than the diameter of the sphere.

$$I_e = I_{e0} [1 + (V_b - V_0)/V_e] \quad (1)$$

I_{e0} is the electron current to the sphere when it is at the potential of the undisturbed plasma: $I_{e0} = C N_e V_e^{1/2} A_b$. The constant C in the formula of Mott-Smith and Langmuir [1926] is $2.68 \cdot 10^{-14} \text{ AmV}^{-1/2}$. N_e is the electron density in m^{-3} . $V_e = kT_e/e$ and A_b is the surface area of the sphere. I_e is a convenient linear function of $(V_b - V_0)$, and will be used for determining the electron current to the electric field probes as well as estimates of the electron current to the Cluster spacecraft.

[9] A conductive spherical body in the magnetosphere will come to a positive potential relative to the undisturbed plasma as a consequence of a current balance between collected electrons and the current of escaping photoelectrons. This is also the situation for the electric field probes. However, it is necessary to bring these probes as close as possible to the potential of the undisturbed plasma, V_{0s} . In the case of Cluster this means as close as possible to V_{np} . This is done by injecting an electron bias current, I_b , to the probes so that the sum of the plasma electron current to a probe, I_{ep} , plus I_b is in balance with the current of photoelectrons escaping from a probe, I_{php} . Based on a number of sweeps of I_b in tenuous plasmas, it was possible to estimate $(V_p - V_{np})$. The detailed procedure is given by Pedersen et al. [2008]. $(V_p - V_{np})$ was found to vary from approximately +2.5 V to +1.5 V from solar maximum to solar minimum for $I_b = 140 \text{ nA}$. A decision to lower I_b to 100 nA in June 2006 did bring the probes to a slightly more positive potential relative to the ambient undisturbed plasma. We will use $(V_p - V_{np}) = (2 \pm 0.5) \text{ V}$ as a sufficient approximation for the probe potential relative to its local plasma. The exact value of this parameter is not critical for high values of $(V_s - V_p)$, but must be considered for calibrations in the solar wind with smaller values of $(V_s - V_p)$.

[10] The Cluster spacecraft has a cylindrical shape, and we need to find an approximation for the collection of electrons. The equipotential surfaces around Cluster in a tenuous plasma will change from ellipsoid-like to spherical with increasing distance from the spacecraft. It is therefore possible to use the electron collection of a sphere, having the same surface area as Cluster, as an approximation. Equation (1) can be used to find the collected electron current, I_{es} , for the Cluster spacecraft as a function of $(V_s - V_{0s})$, by replacing V_b with V_s and V_0 with V_{0s} . The Cluster surface area, $A_s = 23.5 \text{ m}^2$ replaces A_b .

$$\begin{aligned} I_{es} &= C N_e V_e^{1/2} A_s [1 + (V_s - V_{0s})/V_e] \\ &= I_{e0} [1 + (V_s - V_{0s})/V_e] \end{aligned} \quad (2)$$

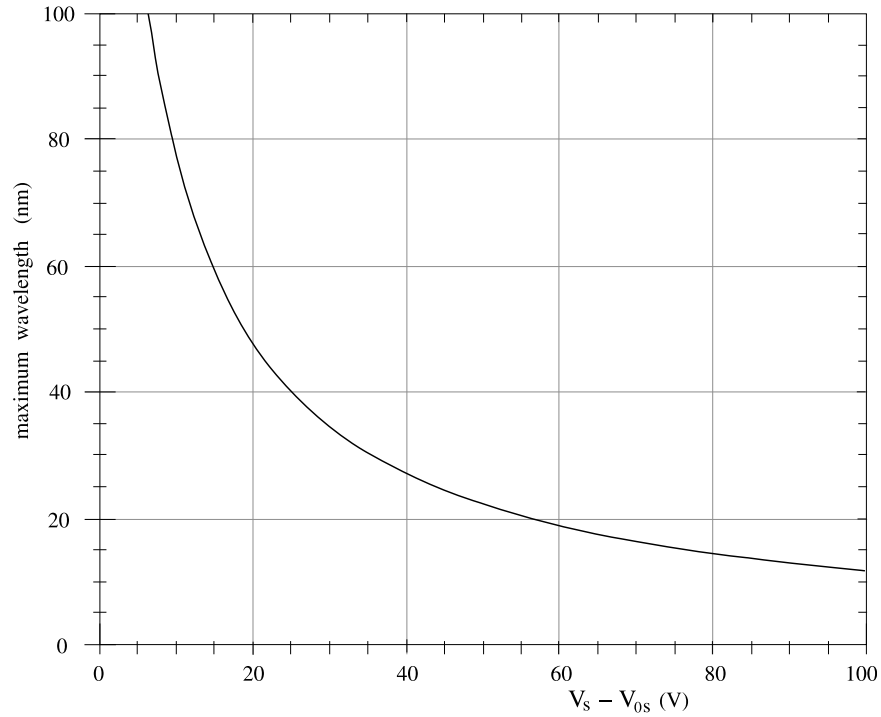


Figure 2. Photoelectrons must have enough energy to first pass the surface work function barrier of (4–6) V, and still have enough energy to overcome the attractive positive potential of the spacecraft, in order to escape to the plasma. The curve shows the maximum photon wavelength (minimum energy) required for producing photoelectrons capable of escaping from a spacecraft at a potential $V_s - V_{0s}$ relative to the undisturbed plasma. In this case the work function has been set to 6 V.

The spacecraft will be at a more positive potential than the electric field probes. It is possible to determine $(V_s - V_{0s})$ when we know the measured parameter $(V_s - V_p)$.

$$\begin{aligned}
 (V_s - V_{0s}) &= (V_s - V_p) + (V_p - V_{np}) + 0.19 (V_s - V_{0s}) \\
 &= (1 - 0.19)^{-1} [(V_s - V_p) + (V_p - V_{np})] \\
 &= 1.23 [(V_s - V_p) + (V_p - V_{np})] \quad (3)
 \end{aligned}$$

I_{es} as a function of $(V_s - V_p)$ can be found by inserting the above equation for $(V_s - V_{0s})$ into equation (2).

[11] The four long EFW booms and the two shorter magnetometer and search coil booms are at the same potential as the central spacecraft body, and have a total area of the order 1.5 m². Long cylindrical elements increase their electron collection as a function of a positive potential bias with a factor $(1 + (V_s - V_{0s})/V_e)^{1/2}$. The booms are not free long cylinders and their electron collection will be in between that of a long cylinder and a sphere. To include their relatively small, but uncertain contribution, we have chosen to set A_s to 25 m².

[12] We will later demonstrate, by calibrations with other Cluster experiments, that the above equations can be used for values of λ_D down to approximately 20 m without significantly changing the N_e estimates we will describe by the use of these equations.

[13] In the following we will determine I_{phs} , the current of photoelectrons escaping from the spacecraft, as a function of $(V_s - V_p)$ by calibrations in the solar wind and in the plasma

sheet. I_{phs} is reduced to smaller values for an increase of $(V_s - V_p)$, and we will demonstrate that I_{es} values of different mean energies in the range (10–100) eV tend to come in current balance with I_{phs} at the same $(V_s - V_p)$ values. The combination of I_{phs} with equations (2) and (3) can be used for estimates of $N_e = N_e(\text{EFW})$ which are nearly independent of electron mean energy as long as it is in the range (10–100) eV. Before we enter into more details on this topic, we will describe how I_{phs} varies with solar EUV radiation during the solar cycle.

3. Solar Photon Energies and Their Photoelectron Energy Distributions

[14] *Feuerbacher and Fitton* [1972] and *Grard* [1973] have analyzed the photoelectron energy distributions from photons with energies up to 20 eV for different materials, including Indium Oxide. On Cluster Indium Tin Oxide was used for giving spacecraft surfaces a conductive coating. These authors found that the main part of the photoelectrons, generated by 20 eV photons, peak at energies well below 20 eV. Similar measurements at higher photon energies have not been carried out. However, it is possible to see what part of the solar spectrum is important for this study. A photoelectron will from the start lose (4–6) eV in crossing the surface work function barrier before leaving the surface, and must still have sufficient energy to pass the positive potential around the spacecraft. Figure 2 shows the maximum photon wavelength (minimum energy) required for producing photoelectrons capable of escaping from a

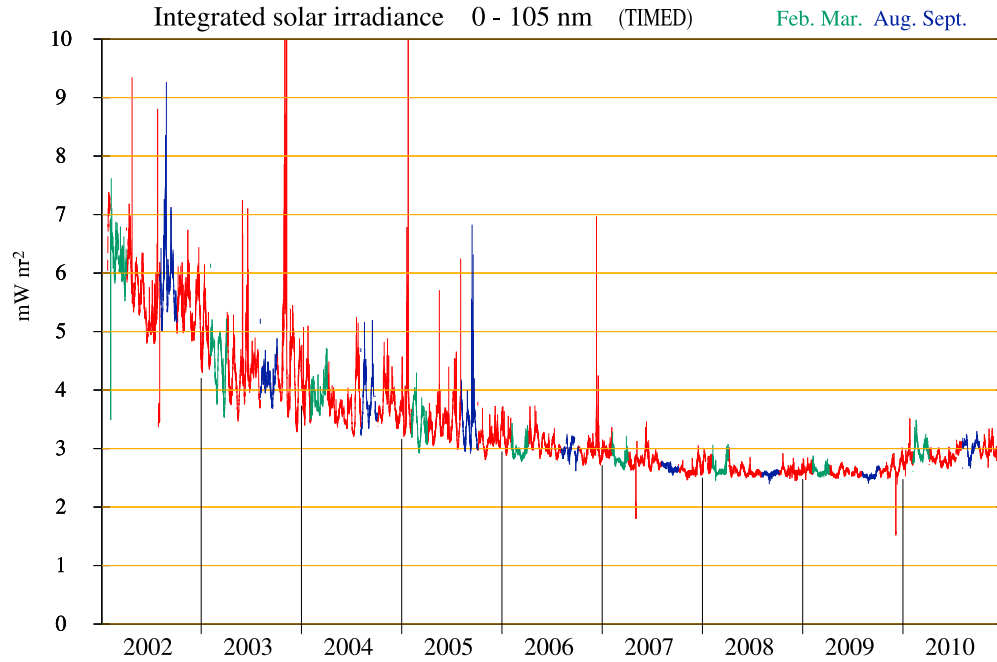


Figure 3. The solar EUV radiation (0–105) nm during the solar cycle from 2002 to 2010 has variations with the solar rotation period. They are more pronounced during solar maximum. A marked drop in the average radiation level has been observed, from near solar maximum to near solar minimum. Green parts are for early in the year (solar wind calibration of method), and blue parts are for early autumn (plasma sheet calibrations).

spacecraft at a potential $V_s - V_{0s}$. The work function is set to 6 V in Figure 2.

[15] Solar radiation data from the TIMED satellite has become available, starting from early 2002.

[16] The integral of the radiation over different wavelengths are given in units of Wm^{-2} in the wavelength range (0–7) nm (7 nm corresponds to 177 eV photons), 0–45 nm (45 nm corresponds to 27.5 eV photons), 0–105 nm (105 nm corresponds to 11.8 eV photons). We will mainly use EUV data covering the latter wavelength range for comparison with variations of I_{phs} , the photoelectron escape current on Cluster. Figure 3 shows the 0–105 nm radiation from 2002 to 2010. The 27 day periodic variations of the EUV radiation, near solar maximum, are clearly related to solar rotations. The mean value of the 0–105 nm radiation at solar minimum is less than 50% of the mean value near solar maximum. The green colored parts are for February–March, when Cluster apogee was in the solar wind, and cross-calibrations with WHISPER were possible. The blue colored parts are for the months of August–September when calibrations in the plasma sheet were possible.

4. Determination of I_{phs} (Current of Escaping Photoelectrons) for Cluster C4 in the Solar Wind

[17] WHISPER is providing very reliable and continuous N_e data in the solar wind. We can determine $I_{\text{es}} = I_{\text{phs}}$ for $(V_s - V_p)$ in the range (6–8) V by having information about N_e and demonstrating that I_{es} is nearly independent of electron energy for these values of $(V_s - V_p)$. A limitation of this calibration is that periods with $(V_s - V_p) = (6–8)$ V only could be carried out for low solar wind plasma densities near 1 cm^{-3} .

[18] Figure 4a shows plots of I_{es}/N_e as a function of $(V_s - V_{0s})$ for the assumed case of Cluster being placed at the ambient plasma potential, and then moved to higher values of $(V_s - V_{0s})$. Using equation (2) we can calculate I_{es}/N_e for $V_e = 5 \text{ V}$, $V_e = 10 \text{ V}$ and $V_e = 20 \text{ V}$, which represent safe limits of V_e in the solar wind. The linear I_{es}/N_e functions, for these values of V_e , tend to focus for $(V_s - V_{0s})$ in the range (10–13) V. We want to relate these I_{es}/N_e values to the measured parameter $(V_s - V_p)$. The shaded areas in Figure 4a define the limits of I_{es}/N_e for $(V_s - V_p)$ of respectively 6 V, 7 V and 8 V. The small spread of I_{es}/N_e is due to the assumed spread of V_e . The limits of $(V_s - V_p)$ reflect the uncertainty in relating $(V_s - V_p)$ to $(V_s - V_{0s})$ because $(V_p - V_{np}) = (2 \pm 0.5) \text{ V}$.

[19] In the solar wind it is necessary to include ion currents, I_{+s} , as a small correction to the current balance of Cluster because of the high velocity of ions in the solar wind. I_{+s} can be estimated as an ion ram current to the projected area, A_r , of Cluster to the solar wind. A_r is approximately 4.5 m^2 , and assuming a range for the solar wind velocity, $v_{\text{sw}} = (300 - 600) \text{ km s}^{-1}$, we can write:

$$I_{+s} = |N_+ e v_{\text{sw}} A_r| = |N_e e v_{\text{sw}} A_r| \quad (4)$$

The ion ram energy of ions is so high that I_{+s} will not vary for the $(V_s - V_{0s})$ values in Figure 4a. We must subtract $I_{+s}/N_+ = (0.2 - 0.4) 10^{-12} \text{ A m}^3$, based on equation (4) (from I_{es}/N_e to get $(I_{\text{es}} - I_{+s})/N_e$ as a function of $(V_s - V_p)$. This function with error bars is presented in Figure 4a. In Figure 4b we use this relation, in combination with WHISPER measurements of N_e , to find $I_{\text{phs}} = I_{\text{es}} - I_{+s}$.

[20] During January–March 2006 the solar EUV radiation was stable at 3 mWm^{-2} . We can in this case find how I_{phs}

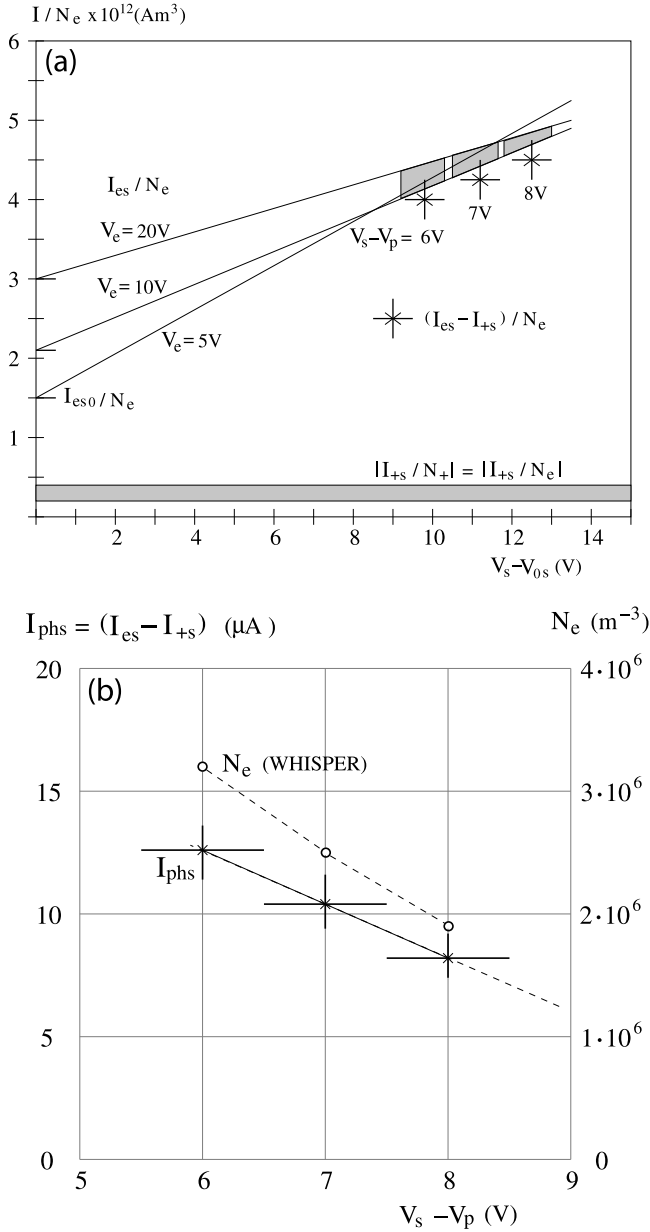


Figure 4. (a) I_{es}/N_e as a function of $(V_s - V_{0s})$ can be calculated for Cluster from equation (2) for different values of V_e . We assume that a safe range for V_e in the solar wind is from 5 V to 20 V. The linear functions of I_{es}/N_e tend to focus near values of $(V_s - V_{0s})$ corresponding to values of $(V_s - V_p)$ in the range (6–8) V. By correcting for a small ion current, I_{+s} in the solar wind, we can find $(I_{\text{es}} - I_{+s})/N_e$, which in turn can be used to find the current of escaping photoelectrons, $I_{\text{phs}} = (I_{\text{es}} - I_{+s})$ when N_e data is available. (b) For January–March 2006 the (0–105) nm solar radiation was stable at 3 mWm^{-2} for longer periods. N_e data from WHISPER, combined with $(I_{\text{es}} - I_{+s})/N_e$ in Figure 4a, could then be used to find I_{phs} versus $(V_s - V_p)$ and demonstrates that I_{phs} increases with approximately 20% per volt when $(V_s - V_p)$ changes from 8 V to 6 V.

varies for $(V_s - V_p)$ between 6 V and 8 V by combining values of N_e from WHISPER, for different solar wind electron densities and $(I_{\text{es}} - I_{+s})/N_e$ in Figure 4a. Figure 4b shows that there is an increase of I_{phs} for $(V_s - V_p)$ from 8 V to 6 V of approximately 20 percent per volt.

[21] Figure 5 shows that the solar EUV radiation in the wavelengths (0–105) nm and (0–7) nm had large variations in the first three months of 2003. Cluster was in the solar wind for a major part of the orbits during this period, and it was possible to find 25 events when $V_s - V_p$ on C4 was at a stable potential between 6 V and 8 V, and N_e from WHISPER could be obtained. In order to compare EUV radiation with I_{phs} based on Figures 4a and 4b, we bring all observations of $(V_s - V_p)$ between 6 V and 8 V to (7 ± 0.5) V, using the slope of I_{phs} in Figure 4b. This resulted in a sufficient number of values of I_{phs} demonstrating the connection between I_{phs} and solar EUV radiation. It also shows that I_{phs} , for $V_s - V_p = (7 \pm 0.5)\text{V}$, varies between approximately $15 \mu\text{A}$ and $20 \mu\text{A}$ during the three months. We will later find $I_{\text{phs}} = I_{\text{es}}$ by calibrations with the electron and ion experiments PEACE and CIS in the plasma sheet during the months August – October. The I_{phs} values obtained from solar wind measurements provide a valuable check of these calibrations.

5. Calibration of $I_{\text{phs}} = I_{\text{es}}$ for Cluster C4 in the Plasma Sheet, the Plasma Sheet Boundary Layer, and the Lobes

[22] Plasma sheet electrons of keV mean energy will provide a current $I_{\text{es}0}$ to the spacecraft nearly independent of the spacecraft potentials we will consider. I_{+s} is a few percent of I_{es} in this plasma, and can be neglected. $I_{\text{es}0}$ can be determined from equation (2) with knowledge of N_e and N_{+} . Different values of N_e (PEACE) and N_{+} (CIS) have been used to determine values of $I_{\text{es}0}$ in balance with I_{phs} at different values of $(V_s - V_p)$. The parallel and perpendicular electron temperature may differ, and it is necessary to find an average value and to avoid situations with large differences in these parameters. Periods with agreement between N_e (PEACE) and N_{+} (CIS) were selected.

[23] To calibrate for small values of I_{es} we must go to the plasma sheet boundary layer, and also to the lobes when PEACE provides electron density and mean energy in this region. We use equations (2) and (3) to find $I_{\text{phs}} = I_{\text{es}}$ as a function of $(V_s - V_p)$ by using N_e and V_e provided by PEACE. The parallel and perpendicular electron temperature may differ, and it is necessary to find an average value and to avoid situations with large differences in these parameters. Periods with a fair agreement between N_e (PEACE) and N_{+} (CIS) were preferred.

[24] Figure 6 presents the result of using selected periods of PEACE data from the Cluster Active Archive (CAA) to find $I_{\text{phs}} = I_{\text{es}}$ (plasma sheet) as function of the measured parameter, $V_s - V_p$, for the years 2001–2006. The scatterplots of I_{phs} have different colors for each year. A logarithmic current scale has been chosen to cover the wide current range. With knowledge of I_{phs} , it is possible to use equations (2) and (3) to calculate the value of $I_{\text{es}} = I_{\text{phs}}$ in the lobes and the polar caps where the electron energies are much lower. In the following we will consider mean electron energies of (10–100) eV. Calculated I_{es} currents for selected

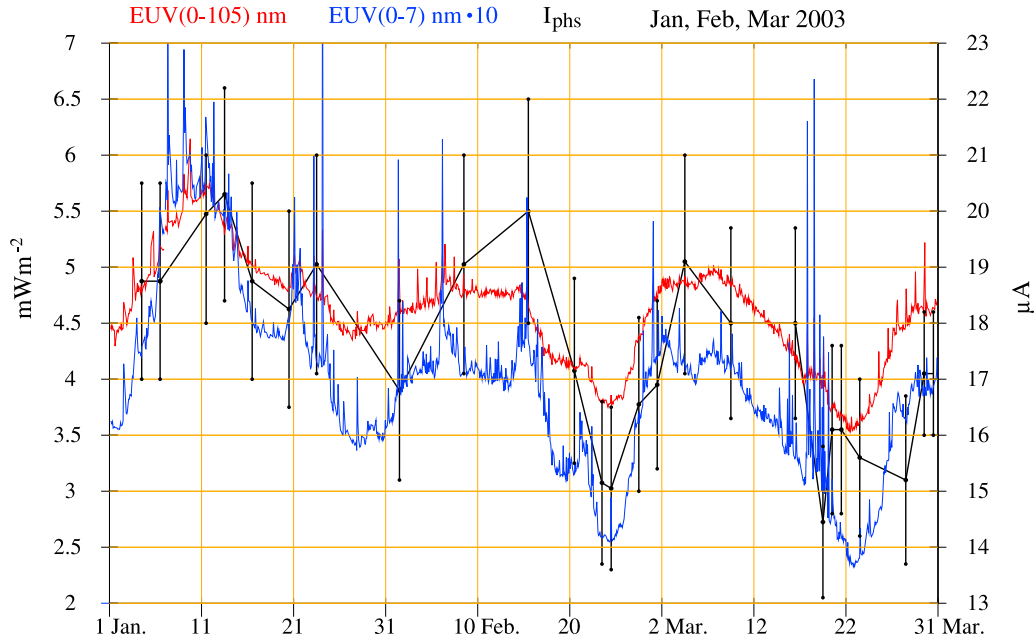


Figure 5. The red curve is the (0–105) nm, and the blue curve the (0–7) nm solar EUV radiation for January–March 2003. $I_{\text{phs}} = I_{\text{es}} - I_{+s}$ for $(V_s - V_p) = (7 \pm 5)$ V is presented for 25 solar wind events when I_{phs} could be determined based on WHISPER measurements. This demonstrates that I_{phs} is controlled by the solar EUV radiation.

values of N_e and $V_e = 10$ V (blue), 50 V (red) and 100 V (black), are drawn as lines in the plots for each year. The crossings of the I_{phs} calibration curves with the model I_{es} curves, based on equations (2) and (3), give estimates of $N_e = N_e(\text{EFW})$ as a function of $(V_s - V_p)$. The I_{phs} color scatterplots for each year is the average of 5–7 events with good data for different values of $V_s - V_p$, and in the first years the spread is probably related to the large variation of EUV radiation with solar rotation. This does not explain the spread in 2005–2006 data, when such variations were small.

[25] The I_{phs} values based on measurements in the solar wind, and their variation with $V_s - V_p$, are also presented in Figure 6. This comparison could first be started in 2002 because very few events with suitable WHISPER and EFW data could be identified at the start of Cluster operations in early 2001. For the first years the error bars are more dominated by solar EUV variations than error bars of the method. Extrapolating I_{phs} values to $V_s - V_p = 8$ V shows that $I_{\text{phs}}(\text{solar wind})$ are in some cases 15–20% lower than I_{phs} from PEACE calibrations. The explanation may be that plasma sheet high energy electrons produce secondary electrons, which add to escaping photoelectrons. The $N_e(\text{EFW})$ technique will mainly be used outside the plasma sheet, and therefore for smaller values of V_e and a more positive spacecraft. Secondary electrons have energies in the eV range and will in this case orbit back to the spacecraft.

We will use the solar wind calibrations, where secondary electrons can be neglected, as the best reference for small values of $V_s - V_p$.

6. Calibrations With PEACE and ASPOC on C3 and WBD on C1

[26] During the autumn of 2003 the four Cluster satellites were separated with a few hundred km in the cusp–polar cap region. Long periods could be identified when all satellites had very similar spacecraft potentials provided that EDI and ASPOC were off and did not influence the spacecraft potential. This demonstrates that the satellites were in the same plasma. Based on this observation it was possible to identify times when ASPOC on C3 was turned on and reduced the spacecraft potential, resulting in $(V_s - V_p)$ of approximately (5–7) V. This made it possible for PEACE to measure a more complete electron spectrum on C3. We can then use $N_e(\text{PEACE})$ on C3 in combination with $(V_s - V_p)$ on C4 to get a calibration of $N_e(\text{EFW})$. Figure 7 presents $N_e(\text{PEACE})$ as a function of $V_s - V_p$ with emphasis on events providing calibrations in a tenuous plasma. The red line has a starting value of $N_e(\text{EFW})$ for $(V_s - V_p) = 30$ V based on the plasma sheet calibration for 2003/2004 in Figure 6.

[27] The black dots and black line, drawn in Figure 7, are derived from a calibration in the northern plasma sheet

Figure 6. The color scatterplots show I_{phs} as a function of $(V_s - V_p)$ from calibrations with PEACE and CIS in the plasma sheet and plasma sheet boundary layer for the years 2001 to 2006. The blue, red and black lines are calculated values of I_e versus $(V_s - V_p)$ based on equations (2) and (3), for selected values of N_e and V_e . Observe that a spacecraft at 30 V near solar maximum will, for the same plasma conditions, be at approximately 20 V near solar minimum. Electron densities as a function of $(V_s - V_p)$ can be estimated from the crossings of scatterplots and colored lines. I_{phs} for $(V_s - V_p) = (6-8)$ V, based on calibrations in the solar wind, are slightly lower than plasma sheet I_{phs} values for the same values of $(V_s - V_p)$.

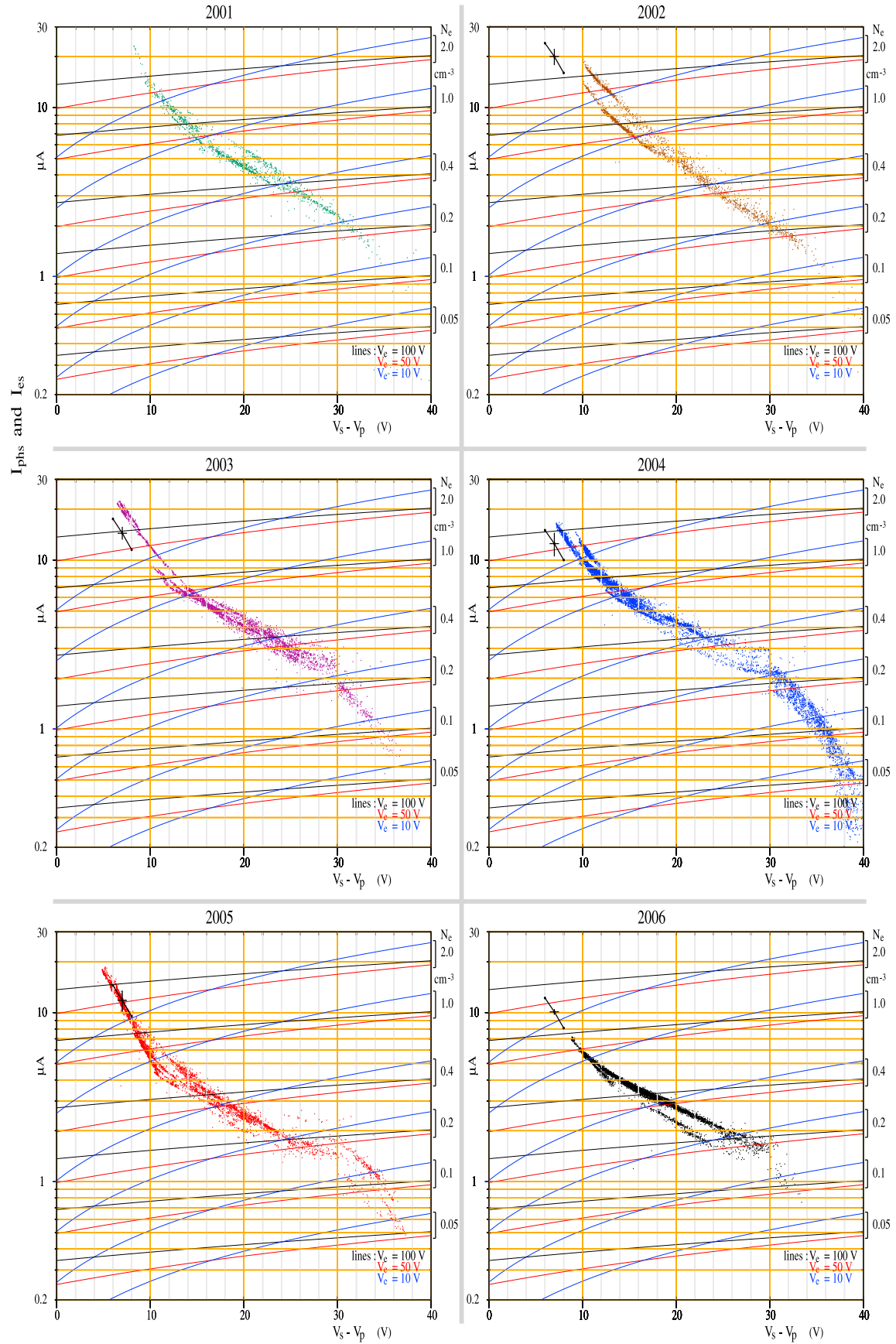


Figure 6

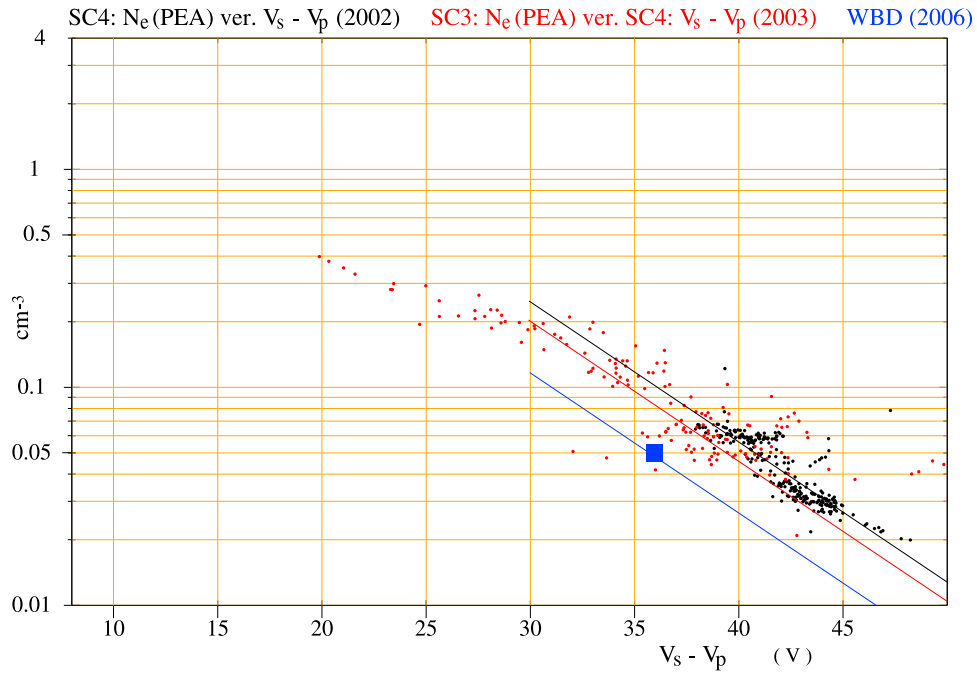


Figure 7. In the autumn of 2003 all Cluster spacecraft were separated by a few hundred km in the cusp-polar cap, and often all spacecraft showed near identical values of $(V_s - V_p)$, indicating that all were in the same plasma. This opened for the possibility to get N_e based on PEACE full spectrum measurements during ASPOC operations on C3, and at the same time get $(V_s - V_p)$ from C4 with no ASPOC operations. The red dots are the result of such measurements during selected periods. The black dots are from a particular event in the lobe in 2002. See Figure 10 and related text. The small square near $(V_s - V_p) = 36$ V is a WBD determination of N_e from a measurement of a cut-off frequency in 2006. The red, black and blue lines are starting at $(V_s - V_p) = 30$ V from N_e values in Figure 6.

boundary layer and lobe in 2002, using CIS and PEACE data (see Figure 10 and related explanations). The starting point for $(V_s - V_p) = 30$ V is also in this case taken from Figure 6.

[28] On 7 September 2006 C1 was in a lobe plasma and WBD observed a low frequency cut-off which could be used to determine the electron density, $N_e = 0.05 \text{ cm}^{-3}$ [Masson *et al.*, 2010]. EDI was operating on C1, and $I(\text{EDI}) = 250 \text{ } \mu\text{A}$ pushed $(V_s - V_p)$ to 50 V, but still allowed WBD wave data to be obtained. A very stable lobe plasma over time, and the observations of very similar values of $(V_s - V_p)$ on C2, within 1000 km from C1, and C4 further out in the lobe, made it possible to conclude that $N_e = 0.05 \text{ cm}^{-3}$ for $(V_s - V_p) = (35.5 - 36.2)\text{V}$ on C4. PEACE measured electron mean energies of 170 eV on C2 and 120 eV on C4. The real values are probably lower, and within the limit for $N_e(\text{EFW})$, because in this case the PEACE spectrum did not cover energies below approximately 50 eV. The blue line, starting from N_e 2005/2006 in Figure 6, and connecting to the WBD calibration near 36 V, provides a calibration of $N_e(\text{EFW})$ for $(V_s - V_p)$ above 30 V for 2006.

7. $N_e(\text{EFW})$ on Cluster C4 as a Function of $V_s - V_p$ From 2001 to 2006

[29] Crossings of the calculated values of I_{cs} , and I_{phs} from plasma sheet calibrations (Figure 6) are used to construct relations between the measured potential, $(V_s - V_p)$ and

$N_e = N_e(\text{EFW})$. The result is presented in Figure 8 as a series of exponential functions covering certain $(V_s - V_p)$ ranges for three periods 2001/2002, 2003/2004 and 2005/2006. $N_e(\text{EFW})$ for the years 2007/2008/2009 is presented in Figure 8 based on the finding that, for a given value of $(V_s - V_p)$, $N_e(\text{EFW})$ changes in proportion to EUV solar radiation. The exponential functions are given in Appendix A. Averages over two, respectively three years are presented because of the relatively small changes within these periods, and considering the uncertainties of the method.

[30] The uncertainty of $N_e(\text{EFW})$ estimates, based on Figure 6, is determined by the spread of I_{phs} calibration values and the differences in calculated I_{cs} values for $V_e = 10$ V, 50 V and 100 V. The spread of this parameter is smallest for $(V_s - V_p)$ between 15 V and 35 V. For low, and particularly for $(V_s - V_p)$ values above 35 V, the spread of I_{phs} is higher.

[31] Figure 7 is making use of some rare opportunities to get N_e data from CIS, PEACE and WBD for $(V_s - V_p)$ above 30 V. In August 2002 C4 passed from the plasma sheet boundary layer to the lobe, see Figure 10. $N_e(\text{PEACE})$ is based on an electron spectrum starting at a few eV, and shows very good agreement with $N_e(\text{CIS})$ based on ion energies high enough not to be retarded by the spacecraft. This data set has also been used to determine $N_e(\text{EFW})$, 2001/2002 for high spacecraft potentials in Figure 8. The only possibility to get the same information for high spacecraft potentials is to shift $N_e(\text{EFW})$ in proportion to solar EUV for the following years. One check on this procedure is provided by $N_e(\text{WBD})$ in the lobe in 2006. This

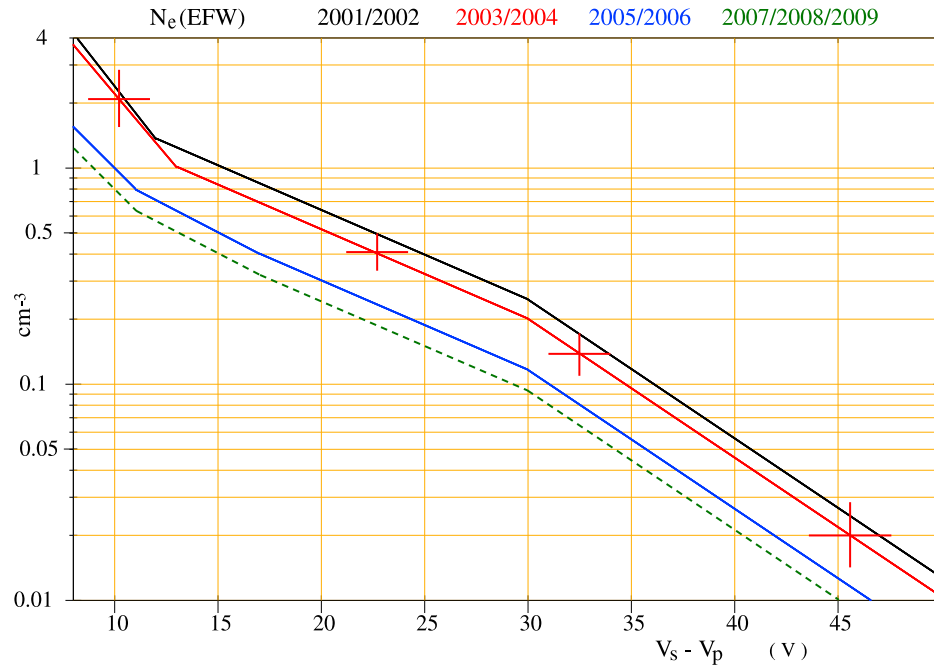


Figure 8. $N_e = N_e(\text{EFW})$ is presented based on data in Figures 6 and 7 for the months of August–September 2001/2002, 2003/2004 and 2005/2006. $N_e(\text{EFW})$ 2007/2008/2009 has been added on the basis of the finding that variations of I_{phs} follow variations of the solar EUV radiation. The error bars marked on the red curve for 2003/2004 are nearly the same for the other periods. Error bars include spread of the photoelectron escape current due to solar EUV variations during solar rotations, and spread due to the range of V_e of (10–100) V used in calculating $I_{\text{es}} = I_{\text{phs}}$.

observation fits in nicely with the $N_e(\text{EFW})$, 2005/2006 curve for $(V_s - V_p)$ above 35 V.

[32] We have chosen to present $N_e(\text{EFW})$, accepting spread caused by solar rotation variations of I_{phs} . It may be possible, but not practical, to reduce the uncertainties by an analysis like the one done for Figure 5. Another possibility is to show different $N_e(\text{EFW})$ curves for different values of V_e . However, this requires accurate knowledge of the electron mean energy. We have chosen to have an independent estimate of the electron density, and show “error bars” for a spread of V_e in the range (10–100) V. $N_e(\text{EFW})$ error bars are approximately $\pm 20\%$ for $(V_s - V_p)$ up to (30–35) V, based on Figure 6. The more uncertain estimates at higher potentials, based on Figures 6 and 7, leads to somewhat higher error bars which are difficult to quantify.

8. Comparing I_{phs} and EUV Solar Radiation During the Solar Cycle

[33] Figure 9 shows the average magnitude and the variation of the EUV solar radiation in the (0–105) nm wavelength range from near solar maximum to solar minimum. Variations with the solar rotation period are pronounced near solar maximum, as can be seen in Figure 3. This means that there can be differences between EUV in the January–March period, where WHISPER solar wind calibrations can be done, and EUV in August–September when PEACE calibrations can be carried out. This is more a concern near solar maximum than for the years near solar minimum, when solar EUV is fairly steady throughout the year.

[34] In order to compare the EUV radiation and PEACE calibration we choose $I_{\text{phs}}(\text{plasma sheet})$ from Figure 6 for $(V_s - V_p) = 20$ V, which is in the middle of the best range for the $N_e(\text{EFW})$ method. Solar EUV and I_{phs} drop with slightly more than a factor 2 from solar maximum to solar minimum. This is more than the drop of Lyman alpha radiation reported by *Brace et al.* [1988].

[35] The reduction of $I_{\text{phs}}(\text{plasma sheet})$ from 2004 to 2005 is larger than the earlier reductions from year to year. The reason may be that the limited numbers of suitable calibration events in 2005 had low EUV levels.

9. $N_e(\text{EFW})$, $N_e(\text{WHISPER})$, $N_e(\text{PEACE})$, and $N_+(\text{CIS})$ in the Lobe, Cusp, and Polar Cap

[36] Figure 10 shows data from the magnetotail when C4 passed from the plasma sheet with mean electron energies near 400 eV, to the boundary layer with increased density and reduced electron energies. PEACE measured a spectrum starting at approximately 5 eV, and CIS measured ions at energies not influenced by spacecraft potential shielding. Between 14:23 UT and 14:43 UT, $N_e(\text{PEACE})$ and $N_+(\text{CIS})$ provides a calibration of $N_e(\text{EFW})$ for 2001/2002 for a wide range of $(V_s - V_p)$. This calibration shows good agreement with the plasma sheet calibration in Figure 6 up to $(V_s - V_p)$ values of approximately 35 V, and in addition provides new calibrations for higher spacecraft potentials. Between 14:43 UT and 14:48 UT, the ion energy dropped so that the spacecraft potential hindered good CIS measurements.

[37] The high plasma density in the boundary layer, shown in Figure 10, is observed for a plasma sheet compression, but

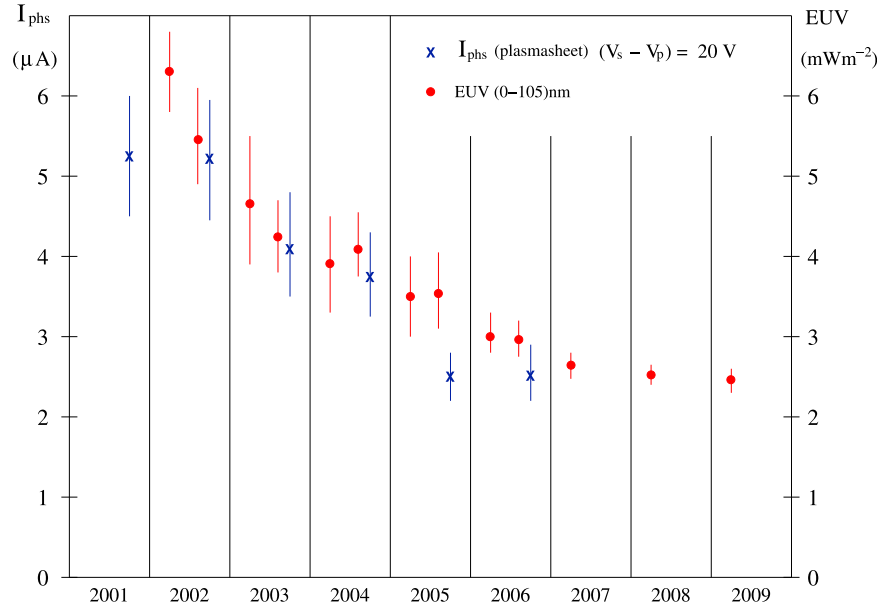


Figure 9. Solar EUV radiation and I_{phs} show very similar reductions from near solar maximum to solar minimum.

is not observed in connection with plasma sheet expansion and the rapid passage of C4 into the plasma sheet. The plasma density gradient, from the boundary layer to the electron density minimum of 0.02 cm^{-3} in the lobe, provides an input to future studies of plasma sheet-lobe dynamics.

[38] A comparison of $N_e(\text{EFW})$ and $N_e(\text{PEACE})$ could be carried out in 2001 for a longer period in a polar cap – lobe plasma at distances of (13–14) R_E . Figure 11 presents data for a special situation when ASPOC is controlling ($V_s - V_{0s}$) to be near 5 V on C3 and C4. $N_e(\text{EFW})$ could be obtained from C1 where ASPOC was not operating. The spacecraft potentials on all satellites were very close to each other before and after ASPOC operations. This indicates that the plasma density was nearly the same on all satellites. Before ASPOC on C3 is turned on, at 11:30 UT, PEACE measured a density of approximately half of $N_e(\text{EFW})$ and a mean energy of approximately 100 eV. There is a fair agreement between $N_e(\text{EFW})$ on C1 and $N_e(\text{PEACE})$ on C3 after ASPOC turn-on C3, resulting in PEACE measuring a more complete spectrum with mean electron energies of (30–40) eV.

[39] Figure 12 shows electron density estimates from EFW, and electron density measurements by WHISPER, for a passage of C4 from the northern cusp, over the polar cap to the plasma sheet boundary layer, on the 2 August 2005. This provides a good opportunity to check $N_e(\text{EFW})$ in the cusp-polar cap. There is very good agreement between $N_e(\text{EFW})$ and $N_e(\text{WHISPER})$ for electron densities above 0.3 cm^{-3} , between 03:30 UT and 05:30 UT. Later the difference between EFW and WHISPER increases as N_e goes to smaller values below 0.2 cm^{-3} . This is a topic for further studies.

[40] It is obvious that PEACE in this case underestimates N_e in the polar cap because the measured spectrum does not cover lower energies. $N_e(\text{CIS})$ could in this case not be measured in the polar cap. The reason must be that ions had

low energies and were reflected by the positive potential of the spacecraft.

[41] However, PEACE and CIS are good references for $N_e(\text{EFW})$ when the full distributions of higher energy electrons and ions were observed in the plasma sheet boundary layer after 08:00 UT. $N_e(\text{EFW})$ is in fair agreement with $N_e(\text{PEACE})$ for electron mean energies up to 100 eV. For higher electron energies of 200–300 eV $N_e(\text{EFW})$ has an overestimate of approximately 50% with reference to $N_e(\text{PEACE})$ and $N_e(\text{CIS})$. This demonstrates the electron energy limit for good $N_e(\text{EFW})$ estimates.

10. $N_e(\text{EFW})$ on C1, C2, and C3

[42] The $N_e(\text{EFW})$ method has been calibrated with PEACE and CIS(CODIF) data from C4 in the plasma sheet and its boundaries. One reason for this choice is the non-operation of EDI on C4. A more serious consideration is the start in 2005 of a gradual development of less positive potentials on the other three satellites when all satellites were in the same steady uniform plasma. This is particularly the case for C3. By 2010 C3 was (8–10)V less positive than C4 at (35–40)V. Furthermore ($V_s - V_p$) on C3 has developed a sinus-like variation at twice the spin frequency with a peak-to-peak variation of 4 V. This difference between C3 and C4 disappears in a more dense plasma when ($V_s - V_p$) is in the range (10–15) V. There is a similar development on C1 and C2 in comparison with C4. However, this amounts to only (1–2) V at high positive potentials.

[43] Early observations in 2001–2002 showed that all Cluster satellites have sinus-like variations at twice the spin frequency with peak-to-peak amplitudes of (0.5–1.0) V when $V_s - V_p$ is in the range (10–20) V. A likely explanation is that a maximum sunlit area of the two short booms ($\sim 0.6 \text{ m}^2$) will occur twice per spin. This area is larger than the sunlit area of the four long booms, which will have a maximum of approximately 0.28 m^2 four times per spin

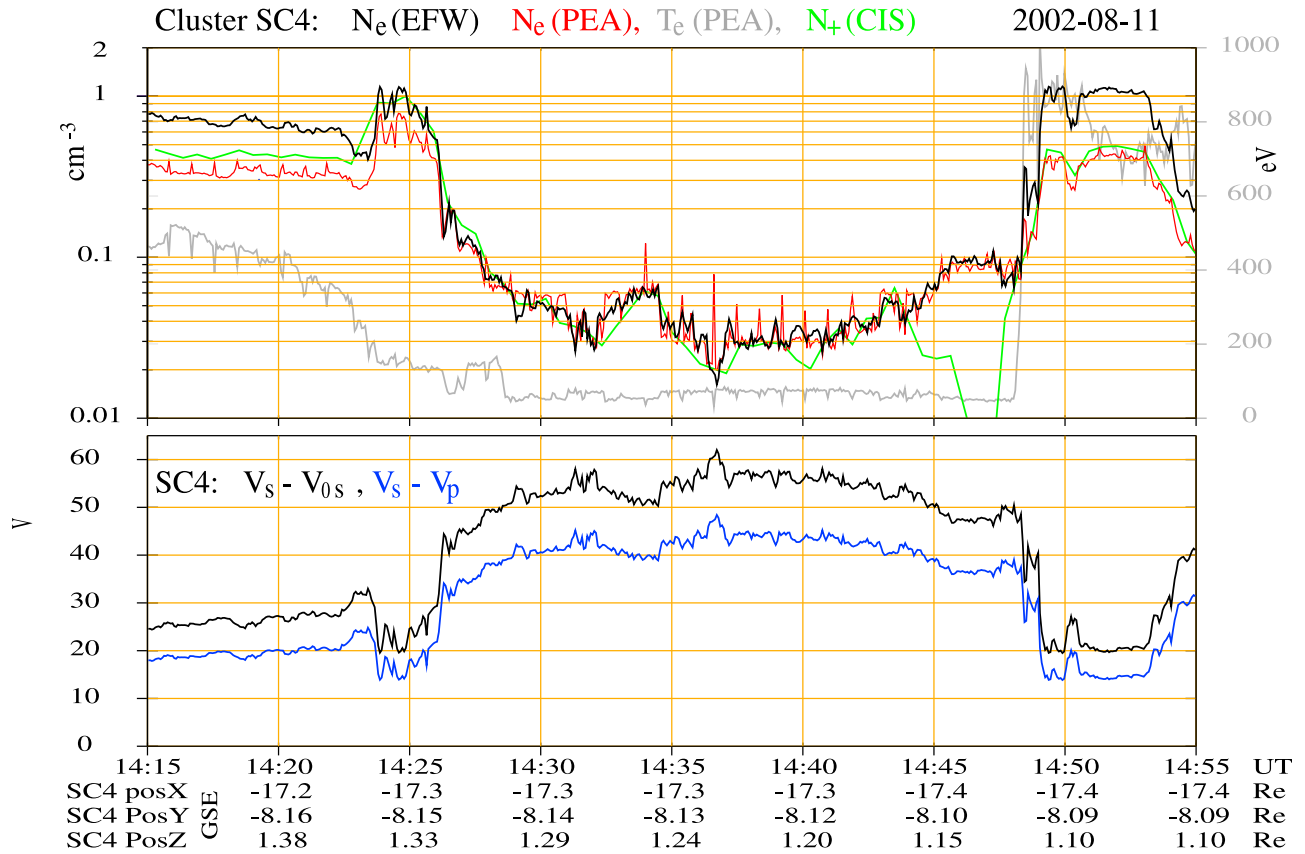


Figure 10. A passage of C4 from the plasma sheet to the boundary layer, and further to the lobe, provides a good opportunity to obtain a calibration of N_e (EFW). PEACE measurements of N_e are based on a complete electron energy spectrum, and the mean electron energy (gray curve in upper panel) is just below 50 eV. The CIS ion measurements are based on relatively energetic ions that could reach Cluster without significant retardation near the spacecraft. This condition does not hold shortly before reentry to the plasma sheet. N_+ (CIS) and N_e (PEACE) are in agreement for the rest of the time in the boundary layer and the lobe. N_e (EFW) is calculated from the exponential functions in Appendix A. The lower panel gives $(V_s - V_p)$, as well as $(V_s - V_{0s})$, the estimated potential between the spacecraft and the plasma at distances beyond spacecraft potential influence.

when the booms are at 45° and 135° relative to the direction to the Sun, and a minimum of approximately 0.2 m^2 in between. For $(V_s - V_p)$ in the range (30–40) V, a sinus-like signal at four times the spin frequency, and with peak-to-peak amplitudes of (1–2) V, was observed. The outer tips of the long booms have a 1.5 m long section biased at -6 V relative to the probes, acting as guards stopping boom tip photoelectrons from reaching the probes. Each guard will have a photoelectron emission of approximately $0.1 \mu\text{A}$ for full solar illumination. Most of these photoelectrons will be attracted back to the spacecraft for very positive potentials. However, a very small fraction may escape to ambient plasma and cause the four times per spin variation, and may also be a small part of I_{phs} at very high spacecraft potentials.

[44] It should be noted that the described spacecraft potential variations do not influence the electric field measurements, which are based on the common mode rejection of the spacecraft potential in the double probe electronics.

[45] V_s is the potential of metal structure which in turn is connected to the conductive coating on the solar cell panels. A large reduction of the spacecraft potential on C3, and smaller reductions on C1 and C2 compared to C4, were

observed after 2005. This may have been caused by loss of surface conductivity of the solar cell coating. Part of the solar cells in shadow will have a smaller positive potential than the rest of the satellite because of absence of photoelectron emission and reduced conductance to other surfaces. This may influence V_s and the measured parameter $(V_s - V_p)$. So far no full explanation has been found for this observation.

11. Summary and Conclusions

[46] Electric field measurements on the Cluster satellites, during a major part of the last solar cycle, have made it possible to determine the potential of the spacecraft and to use this information for electron density estimates in tenuous magnetospheric plasmas. Data from the Cluster electron and ion experiments, and the active wave experiment, WHISPER, and the passive wave experiment WBD, have been used for calibrations of this method. The use of calibrated data from the Cluster Active Archive has greatly facilitated this work.

[47] It was established, from early observations in the magnetosphere, that a spacecraft would be at a positive potential as a consequence of the current balance between

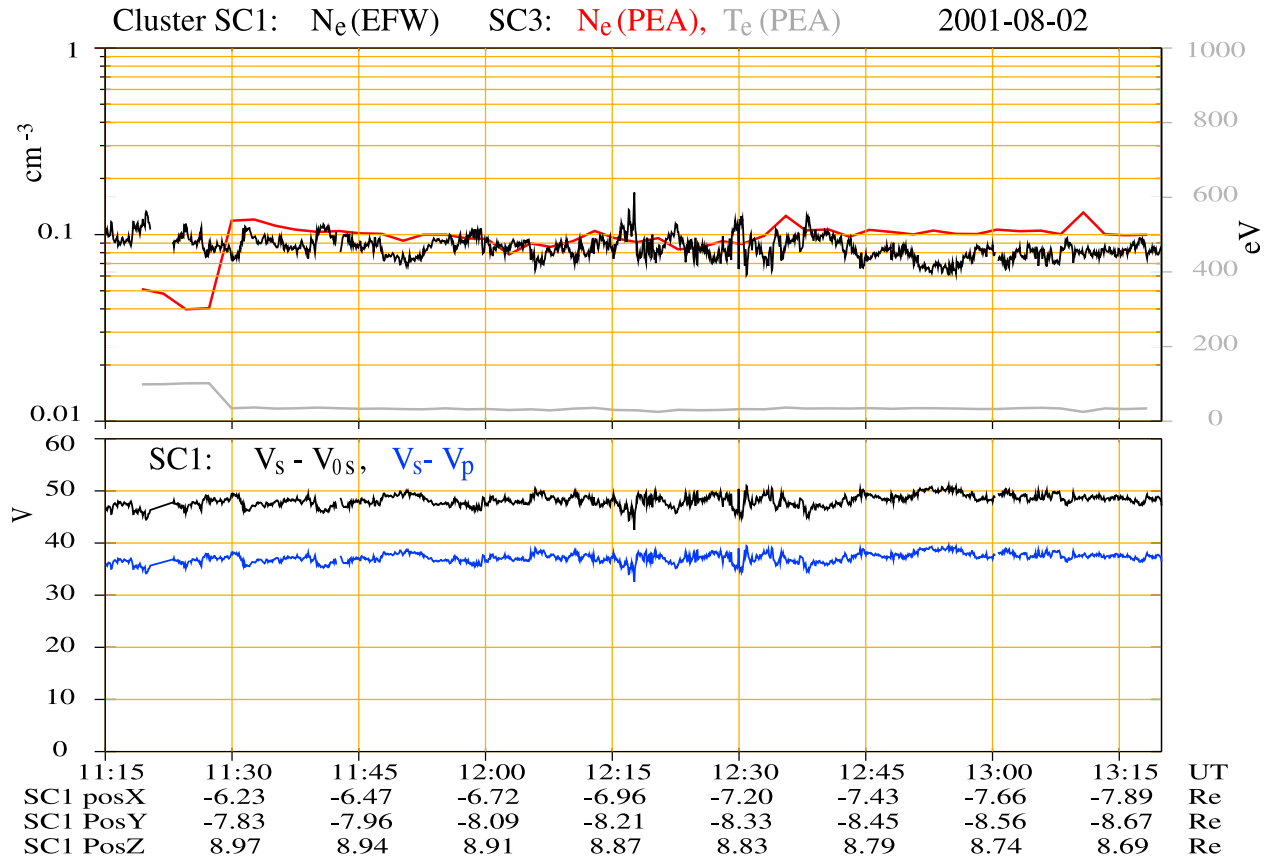


Figure 11. Another opportunity to test N_e (EFW) in a tenuous polar cap – lobe plasma appeared when ASPOC controlled C3 and C4 to be at a potential relative to the ambient plasma of less than 10 V. PEACE could then measure a more complete electron spectrum. C1 had no ASPOC operation. The Cluster satellites were at (13–14) R_E , and all had nearly identical values of $(V_s - V_p)$ before and after ASPOC being active on C3. This indicates that all satellites were in the same plasma during the time period presented, and it is possible to demonstrate agreement between N_e (EFW) on C1 and N_e (PEACE) on C3.

photoelectrons escaping from the spacecraft, and collected ambient electrons. Many papers have been published, describing the use of spacecraft potential measurements for estimating the electron densities. However, variations of photoelectron emission in such estimates were first included in a publication by Pedersen *et al.* [2008]. The present paper, with more data covering the solar cycle, and availability of EUV data from the TIMED satellite, has made it possible to further develop this method and show that the N_e (EFW) method must include changes of photoelectron emission during the whole solar cycle.

[48] The N_e (EFW) method can only be applied for a plasma with a Debye length much larger than the spacecraft. Then it is possible to approximate the electron collection of Cluster with a positive sphere, having a surface area of 25 m^2 . Calibrations of the method in the plasma sheet with data from the electron experiment, PEACE, and the ion experiment, CIS, show that the reduction of photoelectrons from solar maximum to solar minimum will result in a reduction of spacecraft potential for the same plasma conditions. A spacecraft at a potential of 30 V near solar maximum will, for the same plasma conditions, be at a potential of approximately 20 V near solar minimum.

[49] N_e (EFW) is derived from Figure 6, by taking average values of crossings between I_{phs} from calibrations in the plasma sheet and its boundaries, and calculated values of the collected electron current, I_{es} , for different values of N_e and covering a (10–100) eV electron energy range. The best values are obtained for spacecraft potentials between 20 V and 40 V, corresponding to $V_s - V_p$ values of approximately (15–30) V. N_e (EFW) for lower spacecraft potentials will have larger error bars because of the separations of calculated I_{es} curves for $V_e = 10$ V, 50 V and 100 V. We consider that the WHISPER calibrations in the solar wind, free from secondary electrons, are the best calibration for small spacecraft potentials. Measurements of N_e (PEACE) on C3 with ASPOC operating, and simultaneous measurements of $(V_s - V_p)$ on C1 or C4 in the same plasma, has made it possible for a few selected events to calibrate N_e (EFW) for $(V_s - V_p)$ values above 35 V. A similar fortuitous opportunity for calibration was obtained in the plasma sheet boundary layer and the adjacent lobe when PEACE on C4 measured a complete electron spectrum, and N_e and N_+ were in perfect agreement.

[50] Estimates of N_e by EFW in the lobes and the plasma sheet boundary layers are based on good calibrations, and

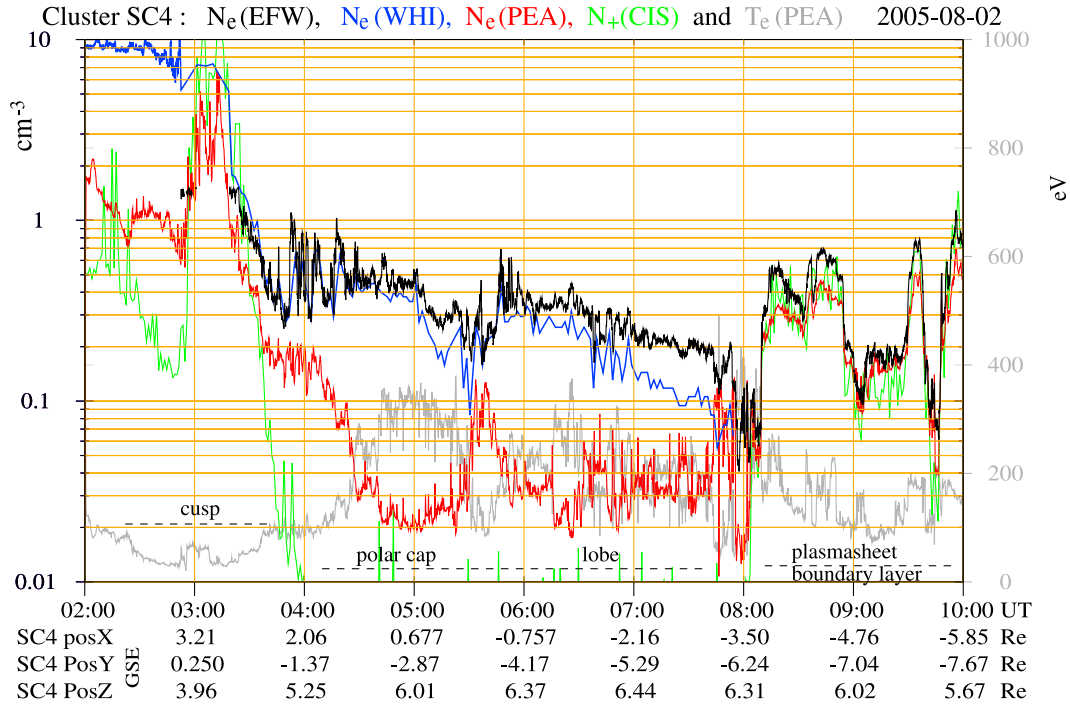


Figure 12. In August 2005 C4 passed the northern cusp, the polar cap – lobe, and entered the northern plasma sheet boundary layer. N_e (WHISPER), blue line, is based on active sounding for electron densities above 0.2 cm^{-3} , and passive wave data for lower electron densities. Other parameters have the same color code as for the previous figures. There is good agreement between EFW and WHISPER for the higher densities, but an increasing difference for lower electron densities. PEACE measures part of the electron spectrum above approximately 40 eV, and underestimates the density. The high electron energies will in some cases cause a small overestimate of N_e (EFW), but not enough to explain the difference with WHISPER. This requires further investigations. N_e (EFW) is in good agreement with N_e (PEACE) when the electron mean energy is near 100 eV in the boundary layer after 09:00 UT.

are useful for situations where PEACE measurements do not cover the lower part of the electron energy spectrum. The same can be said about EFW in a cusp plasma because of the good agreement between EFW and WHISPER as a solid calibration source when using active sounding. The situation is more uncertain in a less dense cusp-polar cap plasma. The difference between N_e (EFW) and N_e from WHISPER passive wave data requires further investigations.

[51] The version of N_e (EFW), published by *Pedersen et al.* [2008] has been used in publications dealing with studies of plasma densities in the lobes [*Svenes et al.*, 2008;

Haaland et al., 2009]. N_e (EFW) in this paper is based on Cluster Active Archive data for calibration of the method and covers a longer period of the solar cycle.

Appendix A

[52] For 2007/2008/2009 the (0–105) nm solar radiation had decreased. To obtain N_e (EFW), each constant A for intervals of $V_s - V_p$ in 2005/2006 must be multiplied with 0.8 (Table A1).

[53] For 2010 the (0–105) nm solar radiation had a small increase. To obtain N_e (EFW), each constant A for intervals of $V_s - V_p$ in 2005/2006 must be multiplied with 0.9.

[54] The above formulas cannot be applied when the spacecraft potential is reduced by ASPOC ion emission, and when EDI electron emission exceeds 80 nA on C1, C2 and C3. EDI does not operate on C4.

[55] **Acknowledgments.** Part of this work has been carried out with support from the Norwegian Research Council. We thank Cluster scientists for access to data via the Cluster Active Archive. We are thankful for access to TIMED EUV data via the NASA open data systems.

[56] Masaki Fujimoto thanks the reviewers for their assistance in evaluating this paper.

References

Brace, L. H., W. R. Hoegy, and R. F. Theis (1988), Solar EUV measurements at Venus based on photoelectron emission from the Pioneer Venus

Table A1. The N_e (EFW) Curves in Figure 8 Can Be Presented as a Series of Exponential Functions

$N_e(\text{EFW}) = A \exp(-U/B)$		
Period	$U = V_s - V_p$ (V)	$N_e(\text{EFW}) (\text{cm}^{-3})$
2001/2002	8–12	$40 \exp(-U/3.55)$
	12–30	$4.3 \exp(-U/10.5)$
	30–50	$20.8 \exp(-U/6.76)$
2003/2004	8–13	$30 \exp(-U/3.83)$
	13–50	$3.5 \exp(-U/10.5)$
	30–50	$17 \exp(-U/6.76)$
2005/2006	8–11	$9 \exp(-U/4.55)$
	11–17	$2.8 \exp(-U/8.75)$
	17–30	$2.03 \exp(-U/10.5)$
	30–50	$9.84 \exp(-U/6.76)$

- Langmuir probe, *J. Geophys. Res.*, 93(A7), 7282–7296, doi:10.1029/JA093iA07p07282.
- Cully, C. M., R. E. Ergun, and A. I. Eriksson (2007), Electrostatic structure around spacecraft in tenuous plasmas, *J. Geophys. Res.*, 112, A09211, doi:10.1029/2007JA012269.
- Décrou, P. M. E., P. Ferreau, V. Krasnosels'kikh, M. Lévêque, P. Martin, O. Randriamboarison, F. X. Sené, J. G. Trotignon, P. Canu, and P. B. Mögensen (1997), Whisper, a resonance sounder and wave analyser: Performance and perspectives for the Cluster mission, *Space Sci. Rev.*, 79, 157–193, doi:10.1023/A:1004931326404.
- Escoubet, C. P., A. Pedersen, R. Schmidt, and P. A. Lindqvist (1997), Density in the magnetosphere inferred from ISEE 1 spacecraft potential, *J. Geophys. Res.*, 102(A8), 17,595–17,609, doi:10.1029/97JA00290.
- Fahleson, U. (1967), Theory of electric field measurements conducted in the magnetosphere with electric probes, *Space Sci. Rev.*, 7, 238–262, doi:10.1007/BF00215600.
- Feuerbacher, B., and B. Fitton (1972), Experimental investigation of photoemission from satellite surface materials, *J. Appl. Phys.*, 43, 1563, doi:10.1063/1.1661362.
- Grard, R. J. L. (1973), Properties of the satellite photoelectron sheath derived from photoemission laboratory measurements, *J. Geophys. Res.*, 78(16), 2885–2906, doi:10.1029/JA078i016p02885.
- Gurnett, D. A., R. L. Huff, and D. L. Kirchner (1997), The wide-band plasma wave investigation, *Space Sci. Rev.*, 79, 195–208, doi:10.1023/A:1004966823678.
- Gustafsson, G., et al. (1997), The electric field experiment for the Cluster mission, *Space Sci. Rev.*, 79, 137–156, doi:10.1023/A:1004975108657.
- Haaland, S., B. Lybekk, K. Svenes, A. Pedersen, M. Förster, H. Vaith, and R. Torbert (2009), Plasma transport in the magnetotail lobes, *Ann. Geophys.*, 27, 3577–3590, doi:10.5194/angeo-27-3577-2009.
- Johnstone, A. D., et al. (1997), PEACE, a plasma electron and current experiment, *Space Sci. Rev.*, 79, 351–398, doi:10.1023/A:1004938001388.
- Laakso, H., and A. Pedersen (1998), Ambient electron density derived from differential potential measurements, in *Measurement Techniques in Space Plasmas: Particles, Geophys. Monogr. Ser.*, vol. 102, edited by E. Borovsky, F. Pfaff, and T. Young, pp. 49–54, AGU, Washington, D. C., doi:10.1029/GM102p0049.
- Laakso, H., R. Pfaff, and P. Janhunen (2002), Polar observations of electron density distribution in the Earth's magnetosphere. Density Profiles, *Ann. Geophys.*, 20, 1725–1735, doi:10.5194/angeo-20-1725-2002.
- Masson, A., O. Santolik, M. G. G. T. Taylor, C. P. Escoubet, A. N. Fazakerley, J. Pickett, A. Åsnes, X. Vallières, H. Laakso, and J.-G. Trotignon (2010), Electron density estimation in the magnetotail: A multi-instrument approach, in *The Cluster Active Archive: Studying the Earth's Space Plasma Environment*, pp. 261–279, Springer, Dordrecht, Netherlands.
- Mott-Smith, H. M., and I. Langmuir (1926), The theory of collectors in gaseous discharges, *Phys. Rev.*, 28, 727–763, doi:10.1103/PhysRev.28.727.
- Nakagawa, T., T. Ishii, K. Tsuruda, H. Hayakawa, and T. Mukai (2000), Net current density of photoelectrons emitted from the surface of the GEOTAIL spacecraft, *Earth Planets Space*, 52, 283–292.
- Pedersen, A. (1995), Solar wind and magnetosphere plasma diagnostics by spacecraft electrostatic potential measurements, *Ann. Geophys.*, 13, 118–129, doi:10.1007/s00585-995-0118-8.
- Pedersen, A., P. Decréau, C. P. Escoubet, G. Gustafsson, H. Laakso, P.-A. Lindqvist, B. Lybekk, A. Masson, F. S. Mozer, and A. Vaivads (2001), Four-point high time resolution information on electron densities by the electric field experiment (EFW) on Cluster, *Ann. Geophys.*, 19, 1483–1489, doi:10.5194/angeo-19-1483-2001.
- Pedersen, A., et al. (2008), Electron density estimations derived from spacecraft potential measurements on Cluster in tenuous plasma regions, *J. Geophys. Res.*, 113, A07S33, doi:10.1029/2007JA012636.
- Rème, H., et al. (2001), First multispacecraft ion measurements in and near the Earth's magnetosphere with identical Cluster ion spectrometry (CIS) experiments, *Ann. Geophys.*, 19, 1303–1354, doi:10.5194/angeo-19-1303-2001.
- Scudder, J. D., X. Cao, and F. S. Mozer (2000), Photoemission current-spacecraft voltage relation: Key to routine, quantitative low-energy plasma measurements, *J. Geophys. Res.*, 105(A9), 21,281–21,294, doi:10.1029/1999JA900423.
- Svenes, K. R., B. Lybekk, A. Pedersen, and S. Haaland (2008), Cluster observations of near-Earth magnetospheric lobe plasma densities—a statistical study, *Ann. Geophys.*, 26, 2845–2852, doi:10.5194/angeo-26-2845-2008.
- Torkar, K., et al. (2001), Active spacecraft potential control for Cluster—implementation and first results, *Ann. Geophys.*, 19, 1289–1302, doi:10.5194/angeo-19-1289-2001.
- Whipple, E. C., Jr. (1965), The Equilibrium Electric Potential of a Body in the Upper Atmosphere and in Interplanetary Space, *Rep. X-615-65-296*, NASA, Greenbelt, Md.

A. N. Fazakerley, Mullard Space Science Laboratory, University College London, Holmbury St. Mary, Dorking RH5 6NT, UK.

S. Haaland, Max-Planck Institut für Sonnensystemforschung, Max-Planck-Strasse 2, D-37191 Katlenburg-Lindau, Germany.

B. Lybekk and A. Pedersen, Department of Physics, University of Oslo, PO Box 1048, N-0316 Oslo, Norway. (bjorn.lybekk@fys.uio.no)

A. Masson and M. G. G. T. Taylor, RSSD, ESA-ESTEC, Keplerlaan 1, NL-2200 Noordwijk, Netherlands.

K. Svenes, Norwegian Defence Research Establishment, PO Box 25, N-2027 Kjeller, Norway.

J.-G. Trotignon, CNRS/LPC2E, 3A av. de la Recherche Scientifique, F-45071 Orléans CEDEX 02, France.